Research Square

Preprints are preliminary reports that have not undergone peer review.
They should not be considered conclusive, used to inform clinical practice,
or referenced by the media as validated information.

Molecular Dynamics Simulations on the Thermal Effect of Interfacial Friction During Asperity Shearing

Zhaoxun Yuan
South China University of Technology
Junxian Zhao
South China University of Technology
Shiping Huang (ctasihuang@scut.edu.cn)
South China University of Technology https://orcid.org/0000-0002-0092-1753

Research Article

Keywords: Interfacial friction, Thermal effect, Friction force, Temperature, Energy, Molecular dynamics

Posted Date: September 24th, 2021

DOI: https://doi.org/10.21203/rs.3.rs-926523/v1

License: This work is licensed under a Creative Commons Attribution 4.0 International License.
Read Full License

Molecular Dynamics Simulations on the Thermal Effect of Interfacial Friction during Asperity Shearing

Zhaoxun Yuan[1], Junxian Zhao[1], Shiping Huang[1,2*]

[1] School of Civil Engineering and Transportation, South China University of Technology, Guangzhou, China

[2] Tsinghua University, State Key Laboratory of Tribology, Beijing, China

Abstract: To explore the thermal effect of interfacial friction at the nano/microscale, a solid-solid contact model of a rough surface with a single peak was established to research single-crystal Fe. The friction characteristics, stress distributions, temperature changes, and energy changes under different indentation depths and lattice orientations during the shearing process were analyzed. From the perspective of temperature and energy, the mechanism of the thermal effect was revealed. The relationship between the friction force, temperature, and energy at the atomic scale was clarified. The results showed that the temperature of the asperities gradually increased during the shearing process, and a stress concentration formed in the shearing zone. After contact, the asperities had undergone unrecoverable plastic deformation, and there was wear at the contact interface accompanied by the loss of atoms from the asperity. At each indentation depth, as the rotation angle of the crystal increased, the friction force, average temperature, and the sum of the changes in thermal kinetic and thermal potential energy all first increased and then decreased; the trends of the three parameters changing with the rotation angle of the crystal were consistent. The average decreases in the friction force, average temperature, and the sum of the changes in thermal kinetic and thermal potential energy were 52.47%, 30.91%, and 56.75%, respectively, for a crystal structure with a rotation angle of 45° compared to a crystal structure with a rotation angle of 0°. The methods used in this study provide a reference for the design of frictional pairs and the reduction of the thermal effect of interfacial friction.

Keywords: Interfacial friction; Thermal effect; Friction force; Temperature; Energy; Molecular dynamics

1 Introduction

Friction is a ubiquitous physical process that exists widely in applications in various fields, such as machinery, civil engineering, and aerospace. The normal operation of most equipment depends on the relative motion between components, and relative motion inevitably causes friction between contact surfaces, which produces thermal effects of friction and mechanical responses. The thermal effect of friction is a very complex process of energy conversion; the most direct impact of the thermal effect of friction is to increase the temperature of the frictional pair. The high local temperature of the contact interface may reach the melting point of the material, resulting in friction-induced failure or interfacial bonding and damage to the structure of the frictional pair in severe cases [1]. Thus, the thermal effect of interfacial friction has become an impediment to analyzing the processes of friction and wear. According to statistics, 1/3-1/2 of the world's energy is consumed by friction in various forms, and wear caused by friction is an important reason for the failure of mechanical equipment. Therefore, reducing the thermal effect of interfacial friction is of great significance for improving the quality of products and prolonging

the service life and increasing the reliability of mechanical equipment.

Research on the thermal effect of interfacial friction mainly includes two aspects: the macroscale and the nano/microscale. Theoretical analyses and experimental measurements are mainly performed on the macroscale [2-5]. However, due to the narrowness of the contact interface, it is not easy to systematically study the temperature distribution between the contact surfaces, and the mechanism of the thermal effect is not completely clear. The friction modes of rough surfaces at the nano/microscale, shown in Fig. 1, include indentation, plowing, and shearing. As a common mode of friction, asperity-asperity shear has become the subject of research to investigate the thermal effect of interfacial friction. All real surfaces are rough surfaces composed of countless asperities with different radii of curvature. This paper has universal significance for the study of the thermal effect of interfacial friction on asperity-asperity contact pairs. Research on the nano/microscale starts from the structure of atoms and molecules. The analysis of the contact and friction behavior of rough surfaces is carried out by molecular dynamics (MD) simulations, which supplements theoretical analyses and experimental measurements and provides a new method to investigate the mechanism of thermal effects and the changes in dynamic microstructure [6-13].

For example, Harrison et al. [14] used MD simulations to analyze the friction produced when two diamond (1 1 1) surfaces are placed in sliding contact; they believed that the mechanical excitation of the interfacial lattice layers (in the form of vibrational and rotational energy) is the essence of friction at the atomic scale. This excitation propagated to the rest of the lattice and eventually dissipated as heat. Chantrenne [15] calculated the energy change for a smooth Au/Au contact pair during sliding friction; their results proved that elastoplastic deformation and adhesion were the main causes of frictional heat. Lin et al. [16] studied the temperature change and microstructure evolution of Cu/Fe and Cu/Ag frictional pairs at different sliding speeds and found that the average temperature for the frictional pair materials increased rapidly with sliding speed. Chen et al. [17] studied the interfacial flow and characteristics of heat transfer during the friction process and showed that the interfacial structure significantly affected the friction force and temperature increase. The atomic flow during the friction process was conducive to heat dissipation and reduced the friction force. In addition, Hayashi [18] studied nanofriction (without wear) between nonmetallic solids. The orderly forced vibration accompanying the sliding motion was separated by sampling and averaging the random thermal motion of passive atoms; they found that the resonance phenomenon significantly increased the energy dissipation rate, resulting in high friction resistance. This results enriched the design theory for sliding parts of high-performance nanoelectromechanical systems (NEMS).

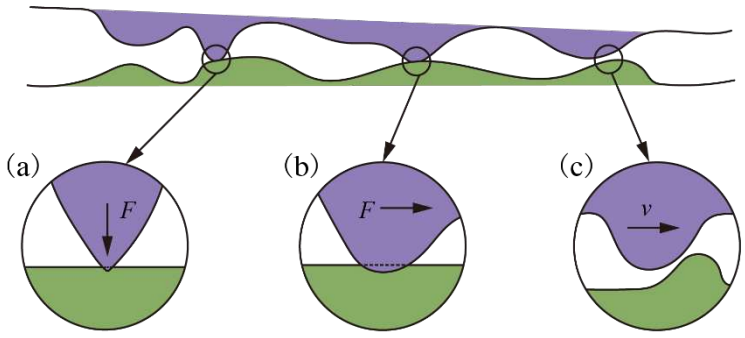

Fig. 1 Friction modes of rough surfaces at the nano/microscale. (a) Indentation. (b) Plowing. (c) Shearing.

To date, much research work has been done on the thermal effect of interfacial friction. Nevertheless, most studies have focused on the relationship between the evolution of the atomic structure of the interface and temperature change. There has been less development of quantitative descriptions and analysis of the thermal effect of interfacial friction from the perspective of microscale energy, and there has been no clarification of the relationship between friction force, temperature, and energy at the atomic scale.

As an indispensable industrial material, Fe is a raw material for producing generators and motor cores, and it is the core component of steel. The durability and performance of Fe materials will be improved by the effective reduction of frictional heat. In this study, single-crystal Fe was taken as the research subject. By changing the indentation depth and lattice orientation, the mechanism of the thermal effect during the shearing of asperities was qualitatively and quantitatively revealed from the perspective of temperature and energy, and the relationship between friction force, temperature, and energy at the atomic scale was systematically clarified. The methods used in this study provide a practical design concept for decreasing the friction resistance and plastic deformation of frictional pairs and reducing the thermal effect of interfacial friction.

2 Methods

2.1 Model Setup

The three-dimensional MD model of asperity-asperity shear is shown in Fig. 2. The model uses Fe with body-centered cubic (bcc) crystal structure, mainly divided into upper and lower parts. Each part is composed of a rigid base and a hemispherical asperity. The rigid base is an Fe plate composed of 6006 atoms, with a size of 55×5×55 Å. An asperity with a radius (R) of 55 Å is connected to the rigid base, with a total of 29932 atoms. The model's size depends on two factors: (1) The model is too small to truly reflect the structural properties on the nano/microscale. (2) The model is too large, and the cost of calculations is too high. In the simulation system, the x-axis oriented in the [1 0 0] lattice direction is consistent with the sliding direction of the asperity. The y-axis oriented in the [0 1 0] lattice direction is perpendicular to the surface of the Fe plate. The z-axis is oriented in the [0 0 1] lattice direction, and the three axes are orthogonal to one other and conform to the right-hand rule. In the model, periodic boundary conditions are imposed along the x-axis and the z-axis, while nonperiodic and shrink-wrapped boundary conditions are imposed along the y-axis. Asperity-asperity shear involves severe elastoplastic deformation, which can easily lead to crystal defects. Compared with the Lennard-Jones (LJ) potential and the Morse potential, the Finnis-Sinclair (FS) embedded-atom method (EAM) multibody potential [19, 20] can better represent the energy and mechanical properties of solid Fe that contains defects. Therefore, this realistic potential is used to simulate the interaction between Fe atoms. The Newtonian equation of motion is solved by the Velocity-Verlet algorithm, and the accuracy of the solution depends on the value of the time step. In the simulation, the time step is 0.001 ps, which not only ensures the accuracy of the simulation but also improves the calculation efficiency. The simulation was carried out with the Larger-scale Atomic/Molecular Massively Parallel Simulator (LAMMPS) MD code.

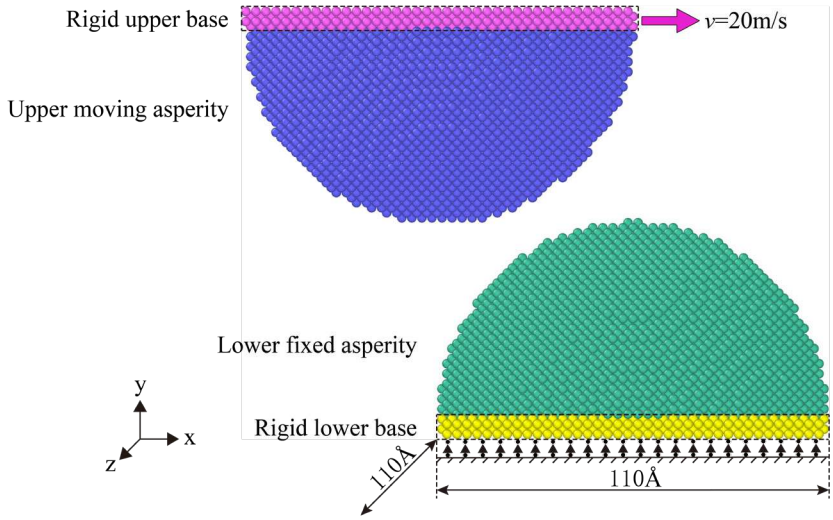

Fig. 2 Three-dimensional MD model of asperity-asperity shear.

2.2 Simulation Process

The simulation process is divided into two stages, namely, the initialization stage and the sliding stage. In the initialization stage, the simulation system fully relaxes and equilibrates at 298 K to ensure that the system has a more reasonable initial configuration. Subsequently, the rigid upper base is slid along the x-axis at a speed of 0.2 ps/Å so that the upper moving asperity and the lower fixed asperity undergo sheared. A sliding speed of 0.2 ps/Å has been widely used in MD simulations of friction and wear [21-24]. Junge [25, 26] and Vadgama [27] showed that the presence or absence of a thermostat in the simulation system has little effect on friction properties such as the tangential action and normal action. To facilitate the quantification of the frictional heat of the interface, the temperature of the system is not controlled during the sliding stage to satisfy the accuracy of the equation of energy balance:

$$W_{sc}(t)=\Delta E_{tot}(t) \tag{1}$$

where $W_{sc}(t)$ is the work done by the friction force during the shearing process of the asperities, and $\Delta E_{tot}(t)$ is the change in total energy in the simulation system.

Due to the shearing between the asperities, energy flows into the simulation system according to the following equation:

$$E_{in}(t)=W_{sc}(t)=\int_0^t F(\tau)v\mathrm{d}\tau \tag{2}$$

where $F(\tau)$ is the friction force at time τ in the shearing process, and v is the sliding speed of the upper moving asperity.

Work done by the friction force leads to an increase in the total energy of the system, and the equation is as follows:

$$\Delta E_{tot}(t)=\Delta E_{kin}(t)+\Delta E_{pot}(t) \tag{3}$$

where $\Delta E_{kin}(t)$ is the change in kinetic energy, which is composed of the change in translational kinetic energy $\Delta E_{kin,tra}(t)$ and the change in thermal kinetic energy $\Delta E_{kin,therm}(t)$. The former does not affect the system's total energy [28, 29], and only $\Delta E_{kin,therm}(t)$ needs to be considered. $\Delta E_{pot}(t)$ is the change in potential energy, which is composed of the change in thermal potential energy $\Delta E_{pot,therm}(t)$ and the change in deformational potential energy $\Delta E_{pot,def}(t)$. The former is caused by the change in atomic arrangement due to the temperature change, and the latter is related to the deformation of the asperities after the upper moving asperity passes over the lower fixed asperity. The latter is derived from the

physical sliding interaction of the asperities, which is an index used to measure the degree of deformation of the asperities after sliding friction.

Notably, the simulation system does not use a thermostat to dissipate the excess energy in the form of heat, so the energy flowing in due to work done by the friction force is stored in the system in the form of kinetic energy and potential energy. In other words, the heat generated by friction is closely related to the increases in the thermal kinetic energy and thermal potential energy [26, 30, 31]. Therefore, to analyze the thermal effect of interfacial friction, the relationship between the work done by the friction force, thermal kinetic energy, thermal potential energy, and deformational potential energy should be clarified.

2.3 Simulation Variables

The influence of two simulation variables, the indentation depth and the lattice orientation, on the friction force, temperature, and energy of the asperity was analyzed. The definitions of indentation depth and lattice orientation are shown in Fig. 3, where γ is the indentation depth, the distance between the bottom of the upper moving asperity and the top of the lower fixed asperity. θ is the rotation angle of the bcc lattice around the z-axis. The values of the simulation variables under each working condition are listed in Table 1. For the indentation depth, the values are 0.00R, 0.02R, 0.04R, 0.06R, 0.08R, 0.10R, and 0.12R, respectively, where R is the radius of the asperity. When friction occurs at the contact interface, the indentation depths mentioned above are similar to the interference range of a single asperity on a rough contact surface [32]. For the lattice orientation, θ is 0°, 9°, 18°, 27°, 36°, and 45°. There are seven indentation depths at each working condition. In this study, a total of forty-two simulations of asperity-asperity shear were carried out.

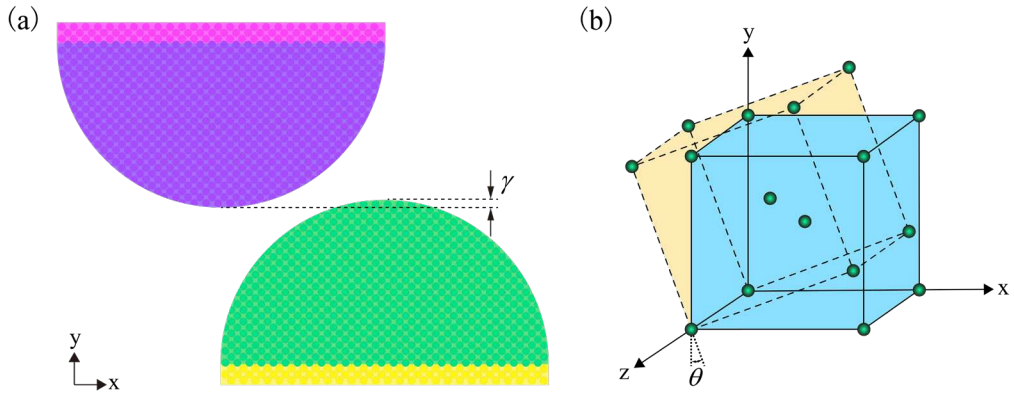

Fig. 3 Definitions of indentation depth and lattice orientation. (a) Indentation depth. (b) Lattice orientation.

Table 1 Values of the simulation variables

Working conditions \ Simulation variables	Lattice orientation	Indentation depth (Å)
I	[1 0 0], [0 1 0], [0 0 1]	0.00R-0.12R
II	[10 63 0], [$\overline{63}$ 10 0], [0 0 1]	0.00R-0.12R
III	[10 31 0], [$\overline{31}$ 10 0], [0 0 1]	0.00R-0.12R
IV	[1 2 0], [$\overline{2}$ 1 0], [0 0 1]	0.00R-0.12R
V	[5 7 0], [$\overline{7}$ 5 0], [0 0 1]	0.00R-0.12R
VI	[1 1 0], [$\overline{1}$ 1 0], [0 0 1]	0.00R-0.12R

3 Results and Analysis

3.1 Friction Characteristics

The thermal effects of interfacial friction directly affect the elastic modulus, hardness, tensile strength, and other physical parameters of materials, thereby indirectly affecting the friction characteristics of the frictional pair [1, 33]. Therefore, friction characteristics are inseparable from the thermal effect of interfacial friction. In the shearing process of asperities, the tangential force (friction force) and the normal force can be obtained by the following equation [27]:

$$\overline{F}_{t/n}=\frac{1}{N}\sum_{i=1}^{N}F_{t/n}(t_i) \tag{4}$$

where $F_t(t_i)$ and $F_n(t_i)$ are the tangential reaction force and the normal reaction force of the rigid lower base at time t_i, respectively. N is the number of times that the reaction forces were evaluated during the shearing process of the asperities. In this study, the reaction forces of the asperities were counted every 500 time steps.

To facilitate the observation and analysis of the change in friction force during the shearing process, the friction force as a function of the normalized sliding distance (x/R) under some working conditions is shown in Fig. 4, where x is the sliding distance of the upper moving asperity. When the upper moving asperity approaches and contacts the lower fixed asperity, the number of atoms in contact increases, and the friction resistance of the upper moving asperity gradually increases from zero. As the indentation depth increases, the time when the upper and lower asperities begin to make contact gradually advances, which is reflected in the normalized sliding distance corresponding to the beginning of contact between the asperities at the four indentation depths in Fig. 4; their values are approximately 0.75, 0.5, 0.375, and 0.25. When the normalized sliding distance is approximately 1.0, the line connecting the centers of the spheres in the upper and lower asperities is nearly parallel to the y-axis, and the friction force at each indentation depth reaches the maximum. After that, as the upper moving asperity continues to slide and passes the lower fixed asperity, the lattice deformation exceeds its limit, causing the lattice atoms to reposition themselves. The pressure in the deformed lattice is released due to the repositioning of the atoms, which is reflected in the slow decline of the friction force from the highest value until it reaches zero. In addition, it can be seen intuitively from Fig. 4 that at each indentation depth, the friction force is smaller when the crystal is rotated by 45° around the z-axis than when the crystal is rotated by 0° around the z-axis, and the sliding distance required for the two asperities to finish the contact is shortened. Notably, violent thermal motion of the atoms of the asperity was generated due to heat produced by friction, and the position coordinates and force states of the atoms were constantly changing, causing the friction force to fluctuate during the shearing process.

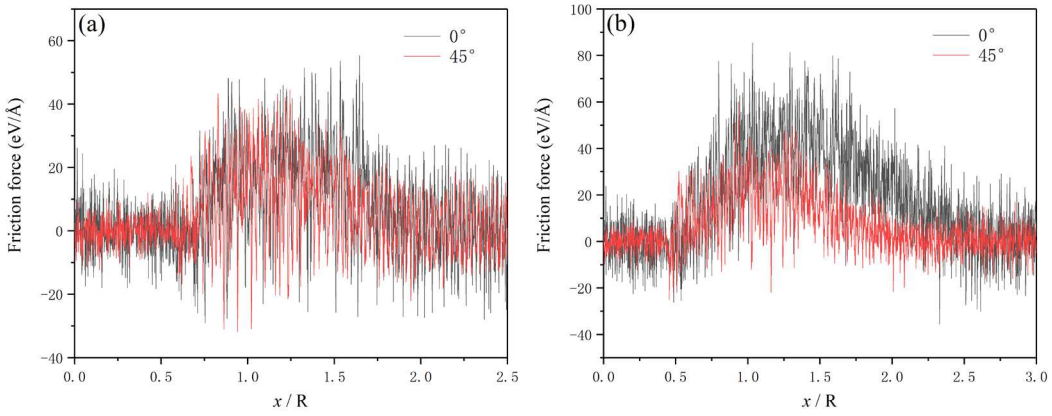

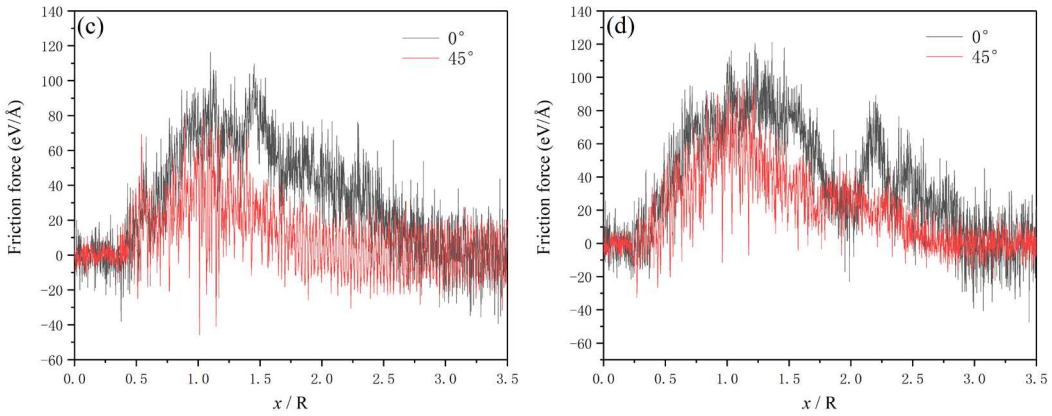

Fig. 4 Friction force as a function of *x*/R under some working conditions. (a) Indentation depth is 0.00R. (b) Indentation depth is 0.04R. (c) Indentation depth is 0.08R. (d) Indentation depth is 0.12R.

The atomic stress (Von Mises) of the asperities under some working conditions is shown in Fig. 5. It can be seen from Fig. 5(b) and Fig. 5(e) that the phenomenon of stress concentration indicated by the arrow appears in the contact area during the contact process, and the maximum atomic stress reaches 46 GPa, which is consistent with the conclusion obtained by Zheng [34]. However, because the contact interface was filled with alkane molecules that provided lubrication, the maximum atomic stress in Zheng's experiment was 40 GPa. In addition to the asperity-asperity shear, similar phenomena, such as indentation, cracking, and bending, were also observed in MD simulations [35-37]. After contact, the elastic deformation of the contact area of the asperities can be restored. Nevertheless, the results showed that unrecoverable plastic deformation remained due to the shearing, and the contact interface was worn and accompanied by the loss of some atoms from the asperity. Compared with Fig. 5(c), the degree of plastic deformation and the number of atoms lost from the asperity in Fig. 5(f) are both lower; the number of atoms lost from the upper moving asperity are 122 and 42, respectively.

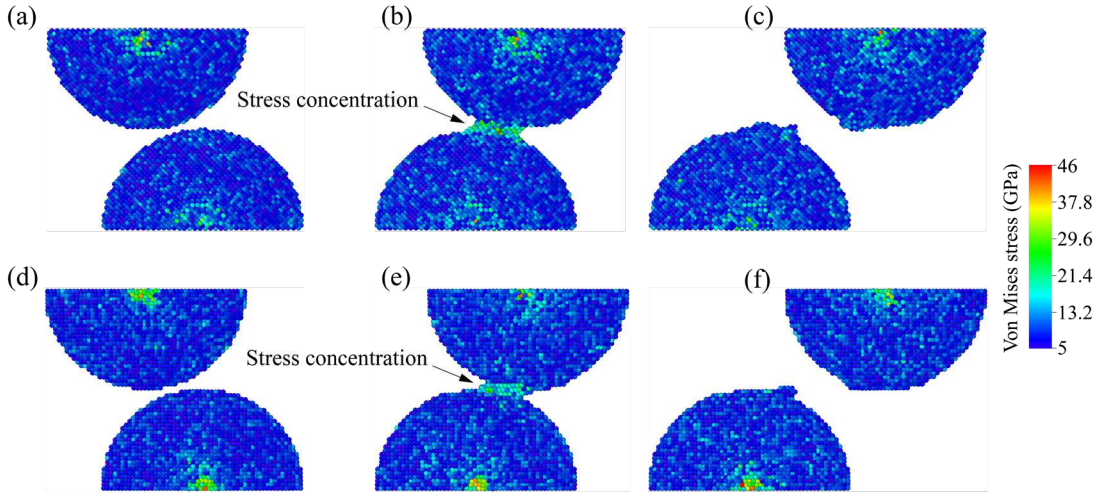

Fig. 5 Atomic stress (Von Mises) of asperities under some working conditions. (a) The indentation depth is 0.00R, and the lattice orientation is 0° before contact. (b) The indentation depth is 0.00R, and the lattice orientation is 0° during contact. (c) The indentation depth is 0.00R, and the lattice orientation is 0° after contact. (d) The indentation depth is 0.00R, and the lattice orientation is 45° before contact. (e) The indentation depth is 0.00R, and the lattice orientation is 45° during contact. (f) The indentation depth is

0.00R, and the lattice orientation is 45° after contact.

The friction force as a function of θ at different indentation depths is shown in Fig. 6. It can be seen from Fig. 6 that except for the indentation depth of 0.12R, as the rotation angle of the crystal increases, the friction force first increases and then decreases. The maximum friction force occurs in the working conditions with a rotation angle of 9° or 18°. For any rotation angle of the crystal, the friction resistance of the asperity increases with the indentation depth, which is consistent with the conclusions obtained by Zhu and Pham [38, 39]. The reason for the above relationship is that the friction force is the sum of the resistances produced by the adhesion effect and the plowing effect [40, 41]. When the indentation depth is greater, more atoms are in contact between the upper moving asperity and the lower fixed asperity, and the upper moving asperity needs to overcome stronger adhesion and displace more atoms during plowing. For the seven indentation depths studied in this article, compared with the working condition with a rotation angle of 0°, the friction force of the crystal structure with a rotation angle of 45° is reduced by 34.12%, 40.82%, 62.71%, 73.01%, 67.23, 52.52%, and 36.91%. The friction force of the crystal structure with a rotation angle of 45° has an average decrease of 52.47%, and the anti-friction effect is more significant than that of other rotation angles. The reason is that when the rotation angle of the crystal is 45°, the sliding surface (1 1 0) is parallel to the direction of movement of the asperity, so the asperity is subject to less friction resistance [42], which is similar to the conclusions obtained by Sorensen [43] and Zhong [29].

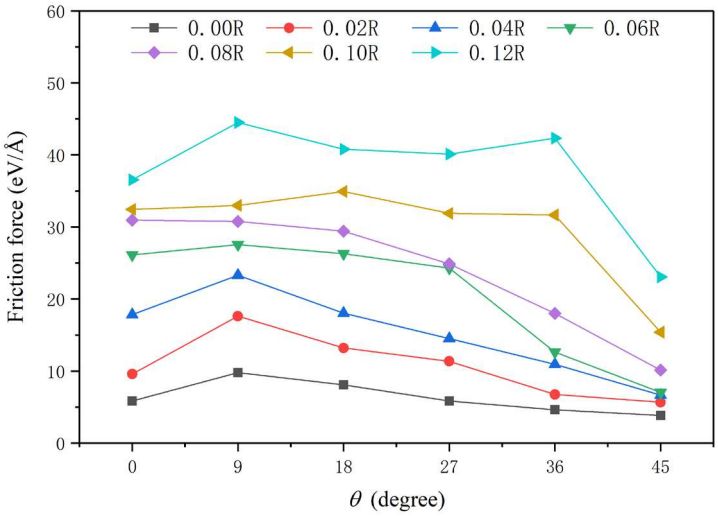

Fig. 6 Friction force as a function of θ at different indentation depths.

3.2 Temperature Changes

The most direct impact of the thermal effect of interfacial friction is increasing the temperature of the frictional pair [44]. The average temperature of the simulation system after contact as a function of θ at different indentation depths is shown in Fig. 7. On the whole, as the rotation angle of the crystal increases, the average temperature of the simulation system after contact first increases and then decreases. The maximum also appears in the working conditions with a rotation angle of 9° or 18°, consistent with the change in the friction force in Fig. 6. For any rotation angle of the crystal, the average temperature of the simulation system after contact increases with the indentation depth. In other words, the indentation depth is positively correlated with the average temperature. At present, research on the thermal effect of interfacial friction rarely analyzes the relationship between indentation depth and average temperature.

Instead, present research only analyzes the influence of sliding speed on average temperature, showing that sliding speed and average temperature are positively correlated [16, 45]. For the seven indentation depths modeled in this article, compared with working conditions with a rotation angle of 0°, the average temperature of the crystal structure with a rotation angle of 45° after contact is reduced by 10.03%, 13.75%, 33.02%, 43.10%, 45.90%, 37.93%, and 32.63%. The average temperature of the crystal structure with a rotation angle of 45° has an average decrease of 30.91%, and the average reduction is larger than that of other rotation angles. The above analysis showed that the crystal structure with a rotation angle of 45° is conducive to reducing the thermal effect of interfacial friction, thereby reducing the temperature of the frictional pair.

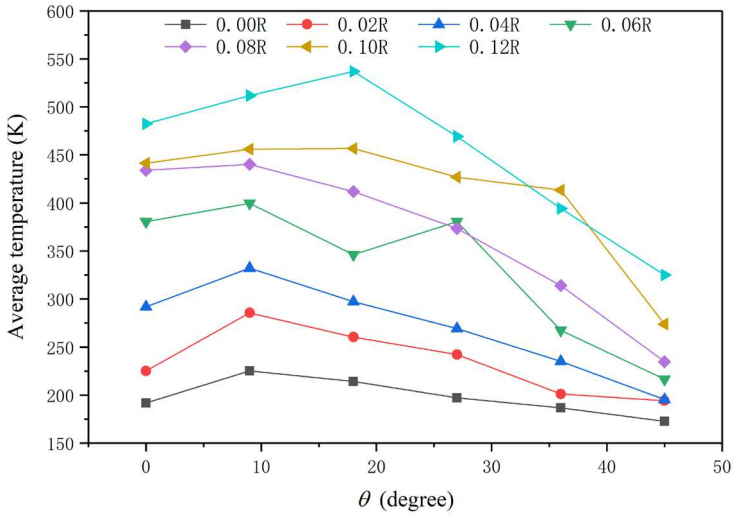

Fig. 7 Average temperature of the simulation system after contact as a function of θ at different indentation depths.

Although the average temperature of the simulation system reflects the strength of the thermal effect of interfacial friction, it cannot explain the temperature distribution of the asperities during the contact process. Therefore, to study the temperature distribution of asperities in the shearing process, the simulation system was divided into 12 layers, from bottom to top, along the y-axis. A single asperity is divided into 5 layers, and the temperature of each layer is calculated every 100,000 time steps. The temperature as a function of the layer number under some working conditions is shown in Fig. 8, where the 0th and 12th layers represent the rigid lower base and rigid upper base, respectively. Because the rigid lower base imposes fixed constraints, and the rigid upper base only performs rigid translational motion, the temperatures of the 0th and 12th layers were zero, according to the relationship between the sum of the kinetic energy of atomic motion and the thermodynamic temperature [33]. The temperature of the asperities in each working condition increases with the normalized sliding distance, which was also concluded by Lin and Chen [16, 17]. In general, the temperature of the 6th or 7th layer before the completion of contact, that is, the temperature in the direct contact area of the asperities before the completion of contact, is slightly higher than that at other positions. After contact, the temperature of each layer of the asperity tends to be the same. When the indentation depth is 0.00R, the crystal structure with rotation angles of 0° and 45° has temperature increments of 56.61 K and 37.09 K, respectively, and the difference in temperature increments is 19.52 K. When the indentation depth is 0.12R, the crystal structure with rotation angles of 0° and 45° has temperature increments of 405.56 K and 222.48 K, respectively, and the difference in temperature increments is 183.08 K. The above results showed that

the difference in the temperature increment increases significantly with the indentation depth. The temperature increment when the crystal is rotated by 45° around the z-axis is smaller than that when the crystal is rotated by 0° around the z-axis., again proving that the crystal structure with a rotation angle of 45° is conducive to reducing the thermal effect of interfacial friction.

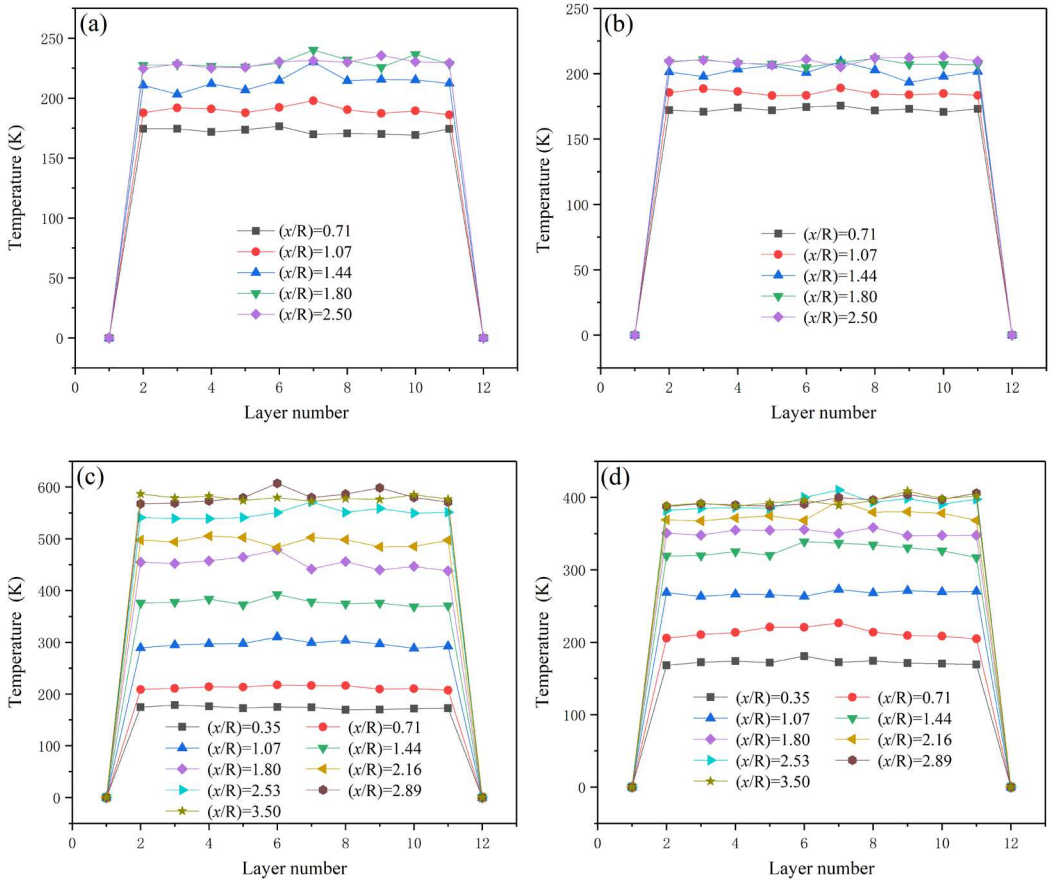

Fig.8 Temperature as a function of the layer number under some working conditions. (a) The indentation depth is 0.00R, and the lattice orientation is 0°. (b) The indentation depth is 0.00R, and the lattice orientation is 45°. (c) The indentation depth is 0.12R, and the lattice orientation is 0°. (d) The indentation depth is 0.12R, and the lattice orientation is 45°.

3.3 Energy Changes

The thermal effect of interfacial friction is a very complex process of energy conversion. When two metals are in contact with each other and strong local shear occurs on the surface, the mechanical energy is converted into heat energy by friction. As mentioned earlier, the heat generated by friction is closely related to the increases in the thermal kinetic energy and thermal potential energy. Therefore, this section analyzes the relationship between the work done by the friction force, thermal kinetic energy, thermal potential energy, and deformational potential energy. To obtain the change in thermal potential energy caused by the temperature change [25, 26], the simulation system is relaxed at 0 K and stabilized at different temperatures. During this process, the upper moving asperity does not slide to prevent the asperities from contacting each other. The equation of thermal potential energy as a function of temperature is obtained by polynomial fitting. Combined with Eq. (3), the change in the deformational potential energy caused by physical sliding interaction can also be obtained.

The energy changes as a function of *x*/R under some working conditions are shown in Fig. 9. It can be

seen from Fig. 9 that when the upper moving asperity gradually approaches and contacts the lower fixed asperity, external energy flows into the simulation system due to the work done by the friction force, as shown by the upward trend in the graph of the change in total energy. At the same time, heat is generated in the friction process, so the graphs of the changes in thermal kinetic and thermal potential energy also show an upward trend, and the change in the thermal potential energy is slightly larger than the change in the thermal kinetic energy. For working conditions (a) and (b) in Fig. 9, the sum of the change in the thermal kinetic energy and the change in the thermal potential energy are 917.26 eV and 619.35 eV, respectively, and the difference between the two is 297.91 eV, indicating that the thermal effect of interfacial friction is weaker when the rotation angle of the crystal is 45° than 0°. The working conditions (c) and (d) in Fig. 9 also reflect the same relationship, and the degree of weakening of the thermal effect is more significant when the indentation depth is 0.12R. The sum of the change in the thermal kinetic energy and the change in the thermal potential energy are 6528.95 eV and 3560.37 eV, respectively, and the difference between the two is 2968.58 eV. Combining the calculation results in Section 3.1 shows that for any indentation depth, the friction force is smaller when the crystal is rotated by 45° around the z-axis than when the crystal is rotated by 0° around the z-axis. Therefore, under the same sliding distance, the crystal structure with a rotation angle of 45° has a smaller change in total energy due to work done by the friction force, and the sum of the change in the thermal kinetic energy and the change in the thermal potential energy is also smaller.

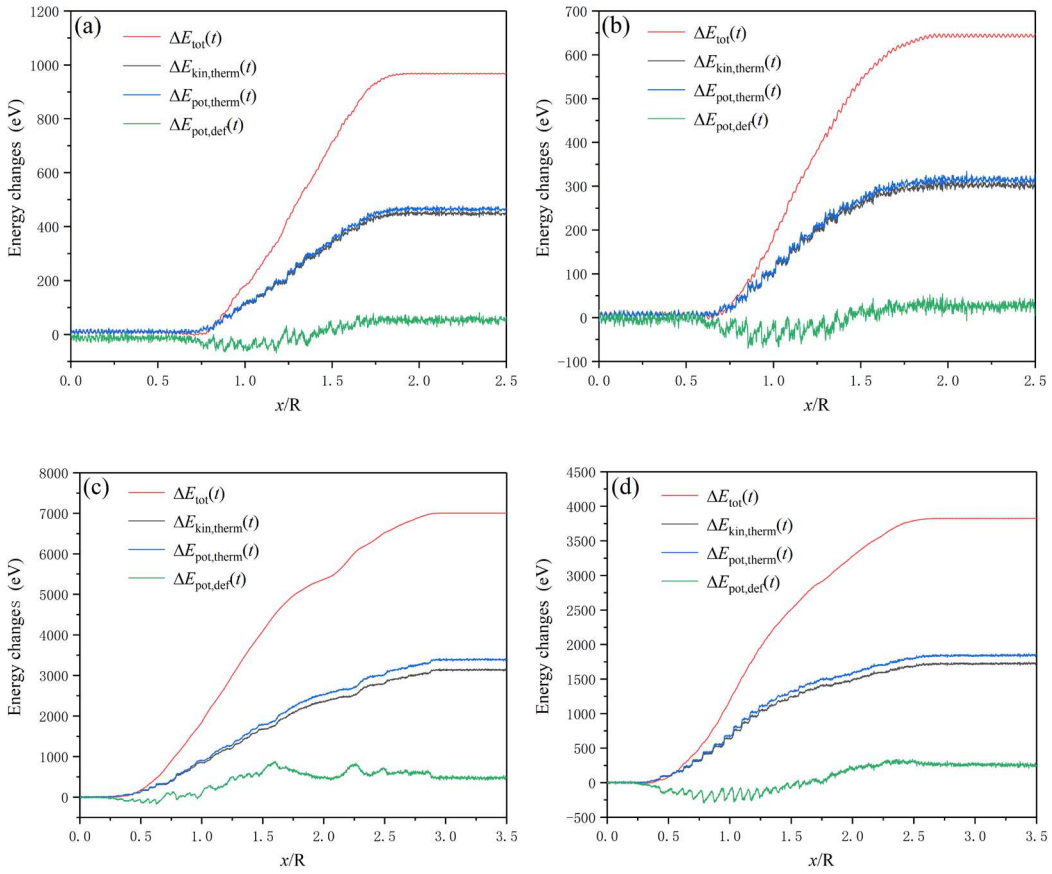

Fig.9 Energy changes as a function of x/R under some working conditions. (a) The indentation depth is 0.00R, and the lattice orientation is 0°. (b) The indentation depth is 0.00R, and the lattice orientation is 45°. (c) The indentation depth is 0.12R, and the lattice orientation is 0°. (d) The indentation depth is 0.12R, and the lattice orientation is 45°.

The sum of the change in the thermal kinetic energy and the change in the thermal potential energy as a function of θ at different indentation depths is shown in Fig. 10. In general, as the rotation angle of the crystal increases, the sum of the change in the thermal kinetic energy and the change in the thermal potential energy first increases and then decreases, which is consistent with the trend in the friction force in Fig. 6 and the trend in the average temperature in Fig. 7. For any rotation angle of the crystal, the sum of the change in the thermal kinetic energy and the change in the thermal potential energy increases with the indentation depth, which is consistent with the conclusion obtained by Junge [26]. For the seven indentation depths used in this article, compared with the working condition with a rotation angle of 0°, the sum of the change in the thermal kinetic energy and the change in the thermal potential energy of the crystal structure with a rotation angle of 45° is reduced by 32.63%, 63.73%, 61.80%, 69.66%, 66.74%, 57.52%, and 45.17%. The sum of the change in the thermal kinetic energy and the change in the thermal potential energy of the crystal structure with a rotation angle of 45° has an average drop of 56.75%, and the average reduction is larger than that of other rotation angles. Combining the calculation results in Section 3.1 and Section 3.2 shows that for the contact pair of asperities on the rough surfaces, as shown in Fig. 2(c), the crystal structure with a rotation angle of 45° (within a reasonable interference range) not only reduces the friction resistance and plastic deformation of the frictional pair but also reduces the temperature increase and heat generated by the thermal effect of interfacial friction.

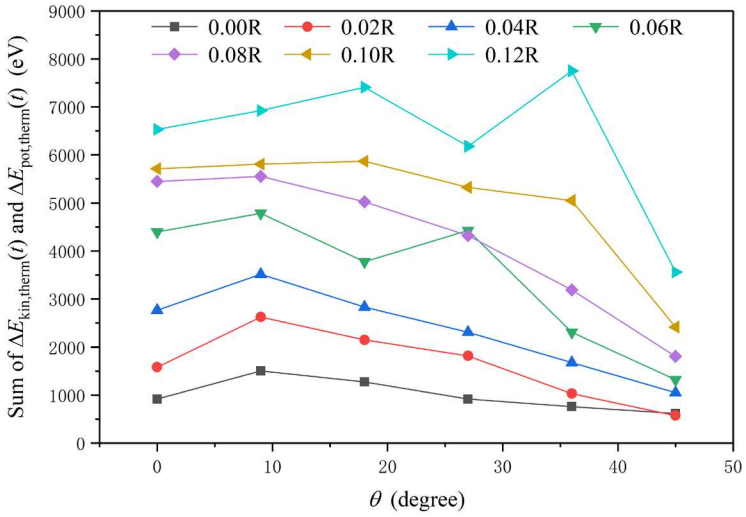

Fig. 10 Sum of the change in the thermal kinetic energy and the change in the thermal potential energy as a function of θ at different indentation depths.

4 Conclusions

In this study, a microscopic contact model of a rough surface with a single peak was established using MD simulations. By changing the indentation depth and the lattice orientation, the mechanism of the thermal effect during the shearing process of asperities was qualitatively and quantitatively revealed from the perspective of temperature and energy, and the relationship among the friction force, temperature, and energy at the atomic scale was systematically clarified. The main conclusions are as follows:

(1) During the shearing process, the temperature of the asperities gradually increased, and violent thermal motion of the atoms was generated due to the heat produced by friction. There was a stress concentration in the shearing zone.

(2) As the number of contact atoms increased and the pressure in the deformed lattice released, the friction force first increased and then decreased. When the indentation depth is greater, the adhesion and

plowing effects are stronger, increasing the friction force. After contact, unrecoverable plastic deformation of the asperities was generated due to shearing. The contact interface was worn and accompanied by the loss of atoms from the asperity.

(3) At each indentation depth, as the rotation angle of the crystal increased, the friction force, average temperature, and the sum of the changes in thermal kinetic and thermal potential energy all first increased and then decreased; the trends of the three parameters changing with the rotation angle of the crystal were consistent. Compared with other rotation angles of the crystal, when the rotation angle is 9° or 18°, the friction force, average temperature, and the sum of the changes in thermal kinetic and thermal potential energy all reach their maximum values, and the thermal effect of interfacial friction is significant. Therefore, the design of such frictional pairs should be avoided.

(4) Compared with the working condition with a rotation angle of 0°, since the sliding surface of the crystal structure with a rotation angle of 45° is parallel to the direction of movement, the average reductions in friction force, average temperature, and the sum of the changes in thermal kinetic and thermal potential energy are 52.47%, 30.91%, and 56.75%, respectively, which dramatically decreases the friction resistance and plastic deformation of the frictional pair and reduces the temperature increase and heat generated by the thermal effect of interfacial friction.

Declarations

Funding This work was supported by the National Natural Science Foundation of China (Grant No. 11672108 and 11911530692).

Conflicts of interest The authors declare that they have no competing interests.

Availability of data and material The raw data can be obtained from the authors upon request.

Code availability The code can be obtained from the authors upon request.

Authors' contributions All authors contributed to the study conception and design. Data collection and analysis were performed by Zhaoxun Yuan and Junxian Zhao and Shiping Huang. The first draft of the manuscript was written by Zhaoxun Yuan and all authors commented on previous versions of the manuscript. All authors read and approved the final manuscript.

Ethics approval Not applicable

Consent to participate Not applicable

Consent for publication Not applicable

References

1. Wen, S.Z., Huang, P.: Principles of Tribology (Fourth Edition). Tsinghua University Press, Beijing (2012)
2. Blok, H.A.: Theoretical Study of Temperature Rise at Surface of Actual Contact Under Oiliness Lubricating Conditions. Proc General Discussion on Lubrication and Lubricants I Mech e. 2, 223-235 (1937).

3. Archard, J.F.: The temperature of rubbing surfaces. Wear. 2, 438-455 (1959). https://doi.org/10.1016/0043-1648(59)90159-0
4. Barber, J.R.: Thermoelastic instabilities in the sliding of conforming solids. Proceedings of the Royal Society A: Mathematical Physical & Engineering Sciences. 312, 381-394 (1969). https://doi.org/10.1098/rspa.1969.0165
5. Bogdanovich, P.N., Tkachuk, D.V.: Temperature distribution over contact area and "hot spots" in rubbing solid contact. Tribology International. 39, 1355-1360 (2006). https://doi.org/10.1016/j.triboint.2005.10.008
6. Maruyama, S.: Molecular dynamics methods in microscale heat transfer. In: Minkowycz W.J., Sparrow E.M. (eds.) Advances in Numerical Heat Transfer, pp. 189-226. Taylor & Francis, New York (2000)
7. Ciraci, S., Buldum, A.: Atomic-scale study of friction and energy dissipation. Wear. 254, 911-916 (2003). https://doi.org/10.1016/S0043-1648(03)00246-1
8. Dias, R.A., Rapini, M., Coura, P.Z., Costa, B.V.: Magnetic friction due to vortex fluctuation. Journal of Applied Physics. 101, 5034-5065 (2007). https://doi.org/10.1063/1.2654067
9. Kim, H.J., Emge, A., Winter, R.E., Keightley, P.T., Kim, W.K., Falk, M.L., Rigney, D.A.: Nanostructures generated by explosively driven friction: Experiments and molecular dynamics simulations. Acta Materialia. 57, 5270-5282 (2009). https://doi.org/10.1016/j.actamat.2009.07.034
10. Huang, S.P., Misra, A.: Micro–Macro-Shear-Displacement Behavior of Contacting Rough Solids. Tribology Letters. 51, 431-436 (2013). https://doi.org/10.1007/s11249-013-0178-y
11. Hu, C.Z., Lv, J.Z., Bai, M.L., Zhang, X.L., Tang, D.W.: Molecular dynamics simulation of effects of nanoparticles on frictional heating and tribological properties at various temperatures. Friction. 8, 531-541 (2020). https://doi.org/10.1007/s40544-019-0271-9
12. Sang, L.V., Yano, A., Isohashi, A., Sugimura, N., Washizu, H.: Friction and Friction Heat of Micronscale Iron. Journal of Tribology. 142, 1-19 (2020). https://doi.org/10.1115/1.4046815
13. Sankar, K.M., Kakkar, D., Dubey, S., Garimella, S.V., Goyat, M.S., Joshi, S.K., Pandey, J.K.: Theoretical and computational studies on nanofriction: A review. Proceedings of the Institution of Mechanical Engineers, Part J: Journal of Engineering Tribology. 234, 448-465 (2020). https://doi.org/10.1177/1350650119863993
14. Harrison, J.A., White, C.T., Colton, R.J., Brenner, D.W.: Investigation of the atomic-scale friction and energy dissipation in diamond using molecular dynamics. Thin Solid Films. 260, 205-211 (1995). https://doi.org/10.1016/0040-6090(94)06511-X
15. Chantrenne, P.: Multiscale simulations: application to the heat transfer simulation of sliding solids. International Journal of Material Forming. 1, 31-37 (2008). https://doi.org/10.1007/s12289-008-0003-6
16. Lin, E.Q., Niu, L.S., Shi, H.J., Zheng, D.: Molecular dynamics simulation of nano-scale interfacial friction characteristic for different tribopair systems. Applied Surface Science. 258, 2022-2028 (2012). https://doi.org/10.1016/j.apsusc.2011.04.117
17. Chen, K., Wang, L.B., Chen, Y.T., Wang, Q.W.: Molecular dynamics simulation of interfaces and microstructure evolution during high-speed sliding. Numerical Heat Transfer; Part A: Applications. 72, 519-535 (2017). https://doi.org/10.1080/10407782.2017.1386513
18. Hayashi, K.: Phononic mechanism determining threshold speed of wearless sliding nanofriction clarified based on molecular dynamics simulations. Computational Materials Science. 188, 1-5 (2020). https://doi.org/10.1016/j.commatsci.2020.110156

19. Mendelev, M.I., Han, S., Srolovitz, D.J., Ackland, G.J., Sun, D.Y., Asta, M.: Development of new interatomic potentials appropriate for crystalline and liquid iron. Philosophical Magazine. 83, 3977-3994 (2003). https://doi.org/10.1080/14786430310001613264
20. Zheng, X., Zhu, H.T., Tieu, A.K., Kosasih, B.: Roughness and Lubricant Effect on 3D Atomic Asperity Contact. Tribology Letters. 53, 215-223 (2014). https://doi.org/10.1007/s11249-013-0259-y
21. Chantrenne, P., Raynaud, M., Clapp, P.C., Rifkin, J., Becquart, C.S.: Molecular dynamics simulations of friction. International Journal of Heat & Technology. 18, 49-56 (2000).
22. Karthikeyan, S., Agrawal, A., Rigney, D.A.: Molecular dynamics simulations of sliding in an Fe–Cu tribopair system. Wear. 267, 1166-1176 (2009). https://doi.org/10.1016/j.wear.2009.01.032
23. Sha, Z.D., Sorkin, V., Branicio, P.S., Pei, Q.X., Zhang, Y.W., Srolovitz, D.J.: Large-scale molecular dynamics simulations of wear in diamond-like carbon at the nanoscale. Applied Physics Letters. 103, 1174-1180 (2013). https://doi.org/10.1063/1.4818713
24. Dai, L., Sorkin, V., Sha, Z.D., Pei, Q.X., Branicio, P.S., Zhang, Y.W.: Molecular Dynamics Simulations on the Frictional Behavior of a Perfluoropolyether Film Sandwiched between Diamond-like-Carbon Coatings. Langmuir. 30, 1573-1579 (2014). https://doi.org/10.1021/la404680v
25. Junge, T., Molinari, J.F.: Molecular dynamics nano-scratching of aluminium: a novel quantitative energy-based analysis method. Procedia IUTAM. 3, 192-204 (2012). https://doi.org/10.1016/j.piutam.2012.03.013
26. Junge, T., Molinari, J.F.: Plastic activity in nanoscratch molecular dynamics simulations of pure aluminium. International Journal of Plasticity. 53, 90-106 (2014). https://doi.org/10.1016/j.ijplas.2013.07.005
27. Vadgama, B.N., Jackson, R.L., Harris, D.K.: Molecular scale analysis of dry sliding copper asperities. Applied Nanoscience. 5, 469-480 (2015). https://doi.org/10.1007/s13204-014-0339-9
28. Balasundaram, R., Jiang, S.Y., Belak, J.: Structural and rheological properties of n-decane confined between graphite surfaces. Chemical Engineering Journal. 74, 117-127 (1999). https://doi.org/10.1016/S1385-8947(99)00063-7
29. Zhong, J., Adams, J.B., Hector, L.G.: Molecular dynamics simulations of asperity shear in aluminum. Journal of Applied Physics. 94, 4306-4314 (2003). https://doi.org/10.1063/1.1558966
30. Mróz, Z., Oliferuk, W.: Energy balance and identification of hardening moduli in plastic deformation processes. International Journal of Plasticity. 18, 379-397 (2002). https://doi.org/10.1016/S0749-6419(00)00103-0
31. Berro, H., Fillot, N., Vergne, P.: Hybrid Diffusion: An Efficient Method for Kinetic Temperature Calculation in Molecular Dynamics Simulations of Confined Lubricant Films. Tribology Letters. 37, 1-13 (2010). https://doi.org/10.1007/s11249-009-9484-9
32. Jackson, R.L., Green, I.: A statistical model of elasto-plastic asperity contact between rough surfaces. Tribology International. 39, 906-914 (2006). https://doi.org/10.1016/j.triboint.2005.09.001
33. Frenkel, D., Smit, B.: Understanding molecular simulation: from algorithms to applications (Second Edition). Academic Press, San Diego (2002)
34. Zheng, X., Zhu, H.T., Kosasih, B., Tieu, A.K.: A molecular dynamics simulation of boundary lubrication: The effect of n-alkanes chain length and normal load. Wear. 301, 62-69 (2013). https://doi.org/10.1016/j.wear.2013.01.052

35. Tanaka, H., Shimada, S., Ikawa, N.: Brittle-ductile transition in monocrystalline silicon ana lysed by molecular dynamics simulation. Proceedings of the Institution of Mechanical Engi neers, Part C: Journal of Mechanical Engineering Science. 218, 583-590 (2004). https://doi. org/10.1243/095440604774202213
36. Xu, S.W., Deng, X.M.: Nanoscale void nucleation and growth and crack tip stress evoluti on ahead of a growing crack in a single crystal. Nanotechnology. 19, 1-15 (2008). https:// doi.org/10.1088/0957-4484/19/11/115705
37. Zhu, P.Z., Fang, F.Z.: Molecular dynamics simulations of nanoindentation of monocrystalline germanium. Applied Physics A. 108, 415-421 (2012). https://doi.org/10.1007/s00339-012-6901-y
38. Zhu, P.Z., Hu, Y.Z., Ma, T.B., Wang, H.: Molecular Dynamics Study on Friction Due to Ploughing and Adhesion in Nanometric Scratching Process. Tribology Letters. 41, 41-46 (2011). https://doi.org/10.1007/s11249-010-9681-6
39. Pham, V.T., Fang, T.H.: Pile-up and heat effect on the mechanical response of SiGe on Si(0 0 1) substrate during nanoscratching and nanoindentation using molecular dynamics. Computational Materials Science. 174, 1-14 (2020). https://doi.org/10.1016/j.commatsci.2019.109465
40. Bowden, F.P., Tabor, D.: The Friction and Lubrication of Solids. Oxford University Press, New York (1950)
41. Hutchings, I., Shipway, P.: Tribology: Friction and Wear of Engineering Materials (2nd Edition). Butterworth-Heinemann, Oxford, U.K. (2017)
42. Giacovazzo, C.: Fundamentals of Crystallography. Oxford University Press, New York (2002)
43. S/rensen, M.R., Jacobsen, K.W., Stoltze, P.: Simulations of atomic-scale sliding friction. Physical Review B. 53, 2101–2113 (1996). https://doi.org/10.1103/PhysRevB.53.2101
44. Li, B., Clapp, P.C., Rifkin, J.A., Zhang, X.M.: Molecular dynamics calculation of heat dissipation during sliding friction. International Journal of Heat & Mass Transfer. 46, 37-43 (2003). https://doi.org/10.1016/S0017-9310(02)00258-2
45. Chen, K., Wang, L.B., Chen, Y.T., Wang, Q.W.: Molecular dynamics simulation of microstructure evolution and heat dissipation of nanoscale friction. International Journal of Heat and Mass Transfer. 109, 293-301 (2017). https://doi.org/10.1016/j.ijheatmasstransfer.2017.01.105